

SCIENTIFIC REPORTS



OPEN

Insights on dramatic radial fluctuations in track formation by energetic ions

Ritesh Sachan¹, Eva Zarkadoula¹, Maik Lang², Christina Trautmann^{3,4}, Yanwen Zhang^{1,5}, Matthew F. Chisholm¹ & William J. Weber^{1,5}

Received: 11 January 2016

Accepted: 16 May 2016

Published: 02 June 2016

We report on unexpected dramatic radial variations in ion tracks formed by irradiation with energetic ions (2.3 GeV ²⁰⁸Pb) at a constant electronic energy-loss (~42 keV/nm) in pyrochlore-structured Gd₂TiZrO₇. Though previous studies have shown track formation and average track diameter measurements in the Gd₂Ti_xZr_(1-x)O₇ system, the present work clearly reveals the importance of the recrystallization process in ion track formation in this system, which leads to more morphological complexities in tracks than currently accepted behavior. The ion track profile is usually considered to be diametrically uniform for a constant value of electronic energy-loss. This study reveals the diameter variations to be as large as ~40% within an extremely short incremental track length of ~20 nm. Our molecular dynamics simulations show that these fluctuations in diameter of amorphous core and overall track diameter are attributed to the partial substitution of Ti atoms by Zr atoms, which have a large difference in ionic radii, on the B-site in pyrochlore lattice. This random distribution of Ti and Zr atoms leads to a local competition between amorphous phase formation (favored by Ti atoms) and defect-fluorite phase formation (favored by Zr atoms) during the recrystallization process and finally introduces large radial variations in track morphology.

For many years, the study of ion track formation by energetic ion irradiation in ceramics has been a subject of interest for materials physicists seeking to understand and improve the radiation tolerance of materials, as well as to utilize the process to create functional/electronic materials due to unique microstructure modifications^{1–3}. Understanding track formation has broad implications for radiation damage for nuclear fuels and waste immobilization^{4,5}, age-dating and thermochronology studies of the earth crust⁶, improving the tolerance of electronic devices to cosmic radiation in space⁷ and fabricating complex nanostructures⁸ for applications, such as fast ion conduction in solid oxide fuel cells^{9,10}. Ion track formation takes place on time scales of 10 to 100 picoseconds, due to inelastic energy loss by energetic ions to electrons and subsequent energy transfer back to the lattice through electron-phonon coupling. The resulting thermal spike causes atomic rearrangement in almost cylindrical channels with nano-sized cross-sections, commonly called ion tracks, along the penetration path of ions in materials.

This work is focused on ion track formation in pyrochlore-structured Gd₂TiZrO₇, which is a widely studied material system due to its interesting physical and chemical properties^{11,12}. Previously, studies have characterized track formation in Gd₂TiZrO₇ induced by swift heavy ions (>~50 MeV) and reported on different aspects, such as track structure, morphology and its dependence on electronic energy-loss, based on different characterization techniques, such as X-ray diffraction (XRD), Raman spectroscopy and transmission electron microscopy (TEM)^{8,13–18}. Among these techniques, XRD and Raman spectroscopy were used to provide macroscopic and averaged information, while TEM results provided atomic scale details^{14,16}. The effect of electronic energy-loss (as well as selection of incident ion and its energy) on the track morphology has been thoroughly discussed. While it is well established that the structure of an ion track in Gd₂TiZrO₇ contains an amorphous core surrounded by a

¹Materials Science and Technology Division, Oak Ridge National Laboratory, Oak Ridge, Tennessee 37831, USA.

²Department of Nuclear Engineering, University of Tennessee, Knoxville, TN, 37996, USA. ³GSI Helmholtzzentrum für Schwerionenforschung GmbH, Planckstrasse, 1, Darmstadt, 64291, Germany. ⁴Materialwissenschaft, Technische Universität Darmstadt, Darmstadt, 64287, Germany. ⁵Department of Materials Science and Engineering, University of Tennessee, Knoxville, TN, 37996, USA. Correspondence and requests for materials should be addressed to R.S. (email: sachanr@ornl.gov)

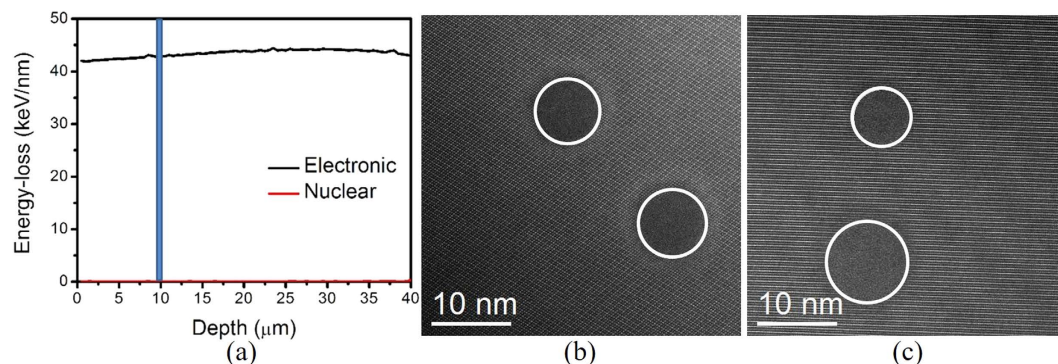


Figure 1. (a) Electronic and nuclear energy-loss 2.3 GeV Pb ions as a function of penetration depth in $\text{Gd}_2\text{TiZrO}_7$. Plan view HAADF images of ion tracks formed by in polycrystalline $\text{Gd}_2\text{TiZrO}_7$ at a depth of $\sim 10\ \mu\text{m}$ showing (b) same and (c) different size track formation. A vertical line drawn in figure (a) at $\sim 10\ \mu\text{m}$ denotes the depth at which ion track image analysis is performed.

concentric defect-fluorite shell layer, the atomic-level details on the local variability in amorphous core diameter and shell-layer thickness have been elusive.

There are a few issues that need to be addressed in order to understand the structural characteristics of ion tracks beyond present knowledge. For instance, it is generally accepted that ion tracks in various $\text{Gd}_2\text{Ti}_x\text{Zr}_{(1-x)}\text{O}_7$ compositions are uniformly cylindrical shaped channels with extremely small variations ($\pm 0.4\ \text{nm}$) in overall track diameter over significantly long track lengths ($\sim 40\ \mu\text{m}$) due to the constant electronic energy-loss from incident ions with $\sim 1\text{--}2\ \text{GeV}$ energy¹⁴. Most TEM investigations have showed coherent images, where details are dominated by thickness, phase and strain contrast. An interpretation of such images is complicated without image simulations and hinders the understanding of actual ion track morphology. Moreover, previous descriptions of track formation have not included the complexity of the recrystallization process and its effect on track morphology. Consequently, any correlative molecular dynamics (MD) simulations and theoretical modeling of ion track formation due to electronic energy loss of ions also become difficult to validate in the absence of quantitative atomic resolution experimental details¹⁹.

In the present work, we provide new insights on the role of recrystallization processes on ion track morphology, through the use of correlated atomic resolution incoherent imaging and MD simulations, that advance the existing knowledge of the subject. We performed nanoscale depth-dependent high angle annular dark field (HAADF) plan view imaging of ion tracks in a 5th order aberration corrected scanning transmission electron microscope (STEM), which provided the incoherent images and ability to three-dimensionally reconstruct an ion track to get morphological information with atomic resolution²⁰. This method has an advantage over cross-sectional TEM imaging, which is limited to qualitative track morphology information. Furthermore, MD simulations, based on the inelastic thermal spike model and two-temperature approach², were conducted to better understand the recrystallization process of ion track formation in $\text{Gd}_2\text{TiZrO}_7$. The MD results are quantitatively consistent with the experimental results. This work provides an improved understanding of the complex nature of energetic ion-lattice interactions and recrystallization process in $\text{Gd}_2\text{TiZrO}_7$ pyrochlore materials by an integrated study of correlative HAADF/STEM and MD simulations.

Results

Electronic (S_e) and nuclear (S_n) energy loss (dE/dx) of 2.3 GeV ^{208}Pb ions in $\text{Gd}_2\text{TiZrO}_7$ pyrochlore, estimated using Monte Carlo simulations in SRIM-2013 code, are shown as a function of ion penetration depth in Fig. 1. Ion track formation is predicted in the material, since S_e energy loss is dominant and well above the threshold for track formation ($\sim 8\text{--}10\ \text{keV/nm}$) throughout the sample thickness of $40\ \mu\text{m}$, while the S_n energy loss is negligible²¹. It is evident from the figure that S_e energy loss remains almost constant at $42\ \text{keV/nm}$ with a variation of less than 5% throughout the sample thickness, which suggests the formation of ion tracks with a constant size and morphology at any depth in the material²². Surprisingly, the experimental observations by HAADF imaging in STEM show an unexpected large variation in size of different ion tracks at the same depth in $\text{Gd}_2\text{TiZrO}_7$ ($\sim 10\ \mu\text{m}$), as shown in Fig. 1(b,c). While two ion tracks of the same diameter of 8 nm are seen in one region of sample, as shown in Fig. 1(b), track diameters are significantly different (7.1 nm and 10.2 nm) in the other region.

To understand the variation in ion track diameter in different tracks in spite of nearly constant S_e energy loss in material, focal series HAADF images were acquired with the electron beam focus changing by 1 nm step into the material. Figure 2 contains HAADF images obtained by focusing at different depths within the specimen, from three different ion tracks in the same sample. The first analyzed ion track is shown in Fig. 2(a–c), where the track diameter is observed to remain unchanged at 7.2 nm throughout the depth of 17 nm. In the second ion track [Fig. 2(e–g)], the track diameter changed from 7.4 nm to 4.5 nm within a track length of 17 nm, which is a change of $\sim 40\%$. In the third ion track [Fig. 2(i–k)], the diameter changes were also large, similar to the second case (from 2.5 nm to 4.8 nm within a track length of 17 nm). However, it is evident from the HAADF images at $f=0, +7$ and $+17\ \text{nm}$ from the surface that this ion track has more radial variations in fractions of amorphous and defect-fluorite phases, unlike the other two cases. A simplified picture of morphology (diameter and length) of all three ion tracks is shown in Fig. 2(d,h,l), illustrating the diametric fluctuations in the ion tracks. The videos

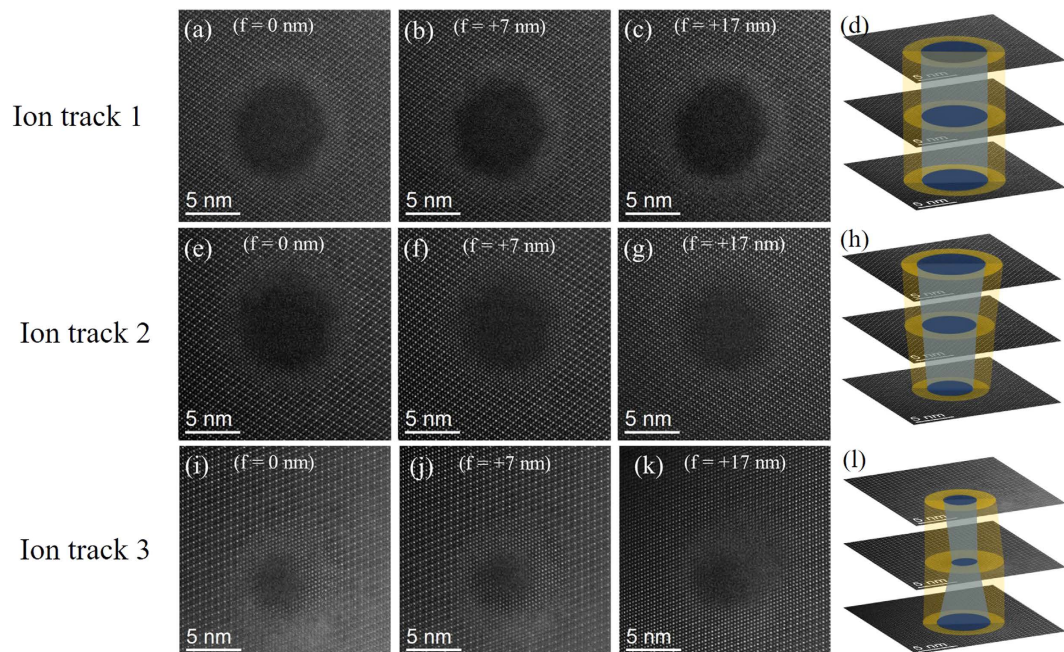


Figure 2. The variation in ion track size and morphology of three different ion tracks within extremely small track length (~20 nm) shown by through-focal series plan-view HAADF images. The through-focal series HAADF images of ion tracks show (a–c) no variation, (e–g) decreasing, and (i–k) abrupt trend change in track diameter. A perspective view of ion track diameter within small depth of ~20 nm is shown in (d,h,l) corresponding to all three ion tracks.

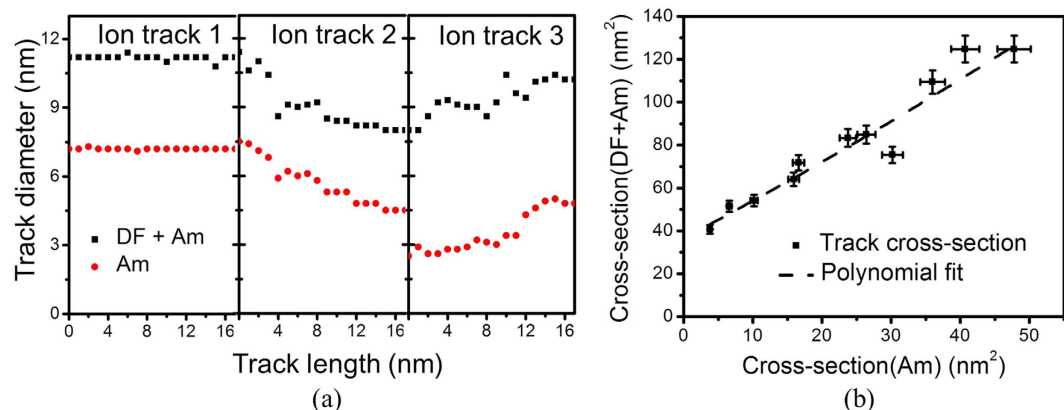


Figure 3. (a) Track diameter as a function of track length, based on the depth dependent HAADF analysis. (b) Total ion track (Amorphous + Defect fluorite) cross-sectional areal dependency as a function of amorphous area in an ion track. A polynomial is fitted to the data points.

of focal series HAADF images acquired by gradually changing the probe focus along the depth in the material are provided in the supplementary section (Video 1, 2 and 3).

So far, we have focused on the variations in the amorphous core of the ion tracks in Gd_2TiZrO_7 . In the next part of the work, the emphasis will be on the core/shell morphology of an ion track, where the defect fluorite phase surrounds an amorphous core in the track as a ring. Based on the depth dependent HAADF analysis of three studied tracks, an analysis of total track diameter as a function of track length is shown in Fig. 3(a). The thickness of the defect-fluorite phase layer is 5–6 atomic layers, i.e. ~1.5–2 nm, and remains constant irrespective of the size variations in the amorphous core of the ion track. An exception can be seen in case of ion track 3 in Fig. 2, where the variation of the defect-fluorite phase thickness is due to more dramatic diametric fluctuations of tracks. A plot of total track cross-section (defect fluorite + amorphous) is shown in Fig. 3(b) as a function of amorphous core cross-section. A polynomial fit of the form, $y = 0.0056x^2 + 1.66x + 37.3$, describes the total cross-section (y) dependence on the amorphous core cross-section (x).

To understand the evolution of diametric fluctuations in ion track formation in Gd_2TiZrO_7 , MD simulations as a function of time are performed, as shown in Fig. 4. The figure shows only the interstitials formed during

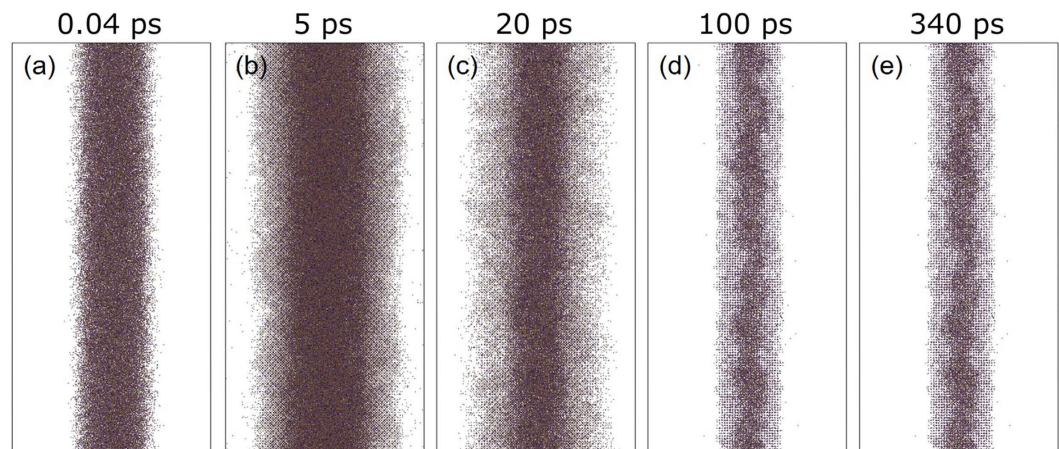


Figure 4. Molecular dynamics simulations of the time evolution of an ion track in $\text{Gd}_2\text{TiZrO}_7$. For clarity, only the interstitials are shown in the figure, white background represents the ordered atomic structure. The figure illustrates the interstitials formed in $\text{Gd}_2\text{TiZrO}_7$ after simulation times of (a) 0.04, (b) 5, (c) 20, (d) 100 and (e) 340 ps. In the intermediate stages of the recrystallization process, interstitials are formed in a larger region than the melt zone of the ion track due to energy transfer to lattice atoms (at 5 and 20 ps). In the final stages of the recrystallization, the diametric variations are evident in the ion track.

the process for better visual clarity. The initial super-heated melt zone of the thermal spike is shown in Fig. 4(a). This thermal spike induces a shock wave and ejects interstitials into the surrounding matrix, and the melt zone expands into the surrounding matrix, even while the superheated track core cools, as shown in Fig. 4(b). As the molten track core cools further (Fig. 4(c)), interstitials in the ordered pyrochlore matrix begin to relax and epitaxial crystallization of the disordered defect fluorite structure is initiated at the melt-crystalline interface. In the later stages of cooling and crystallization, the defects in the ordered pyrochlore structure mostly recover, the crystallization of the defect fluorite structure ceases, and the remaining molten core quenches to an amorphous structure. This results in an ion track with an amorphous core and defect fluorite shell structure that exhibits significant diametric fluctuations in the core-shell morphology, as shown in Fig. 4(d). The simulations were run for longer time (~ 340 ps), even after the completion of the track recrystallization, to ensure the stability of track morphology, as shown in Fig. 4(e). From the simulations, it is clear that the observed dramatic diametric variations in the tracks emerge during recrystallization of the molten track containing two very different B-site cations. Figure 5(a) illustrates a slice of recrystallized ion track in $\text{Gd}_2\text{TiZrO}_7$ after 340 ps of simulation time along the track length, where the variations of the ion track diameter are clearly evident. The ion track consists of an amorphous core, and a defect-fluorite shell structure, in agreement with the experimental findings discussed above. The sectioned images of ion track at two different depths (indicated in Fig. 5(a)) are presented in Fig. 5(b,c). These results clearly illustrate significant change in track diameter over a short increment of track length. To understand the track recrystallization process further, MD simulations were also performed under similar conditions for $\text{Gd}_2\text{Ti}_2\text{O}_7$ as shown in Fig. 5(d), where the formed track is observed with rather uniform diameter. Likewise, ion tracks in $\text{Gd}_2\text{Zr}_2\text{O}_7$, which are composed of completely crystallized defect fluorite structure (i.e., no core shell structure), exhibit weak strain contrast and no evidence for significant diametric variation⁸. Bright field (BF) cross-sectional images of the tracks in $\text{Gd}_2\text{TiZrO}_7$ and $\text{Gd}_2\text{Ti}_2\text{O}_7$ are shown in Fig. 5(e,f), respectively, which give a projected view of the tracks embedded in the crystalline matrix. The images demonstrate the larger diametric variations for the tracks formed in $\text{Gd}_2\text{TiZrO}_7$, as compared with tracks in $\text{Gd}_2\text{Ti}_2\text{O}_7$. Despite the agreement in the core diameter variation, there is some discrepancy between the experimental and the MD results regarding the shell size variation, which in the experiments is not significant. This discrepancy could be attributed to the deficiencies in the interatomic potential, or due to further relaxation processes that occur over the longer time scales of the actual irradiations or the time between irradiation and characterization, and it is not possible to capture such processes in the MD simulations.

Discussion

Since the electronic energy loss by ions in a material is somewhat stochastic in nature, irrespective of the target material, the morphological difference in track formation in $\text{Gd}_2\text{TiZrO}_7$ and $\text{Gd}_2\text{Ti}_2\text{O}_7$ is primarily attributed to the random distribution of Ti and Zr atoms on the B-site of the $\text{Gd}_2\text{TiZrO}_7$ pyrochlore structure. Because of the differences in electron densities and ionic radii for Ti and Zr, local energy dissipation, electron-phonon coupling, and epitaxial crystallization processes are all affected. The ionic radius of Zr is larger than that of Ti ($r_{\text{Ti}} < r_{\text{Zr}}$) and similar to that of Gd. As a result, the presence of Zr in the pyrochlore structure favors the formation of the defect-fluorite phase during track crystallization due to its low formation energy. On-the-other-hand, the defect fluorite structure is unstable for the small ionic radius of Ti, and $\text{Gd}_2\text{Ti}_2\text{O}_7$ favors formation of the amorphous phase under track formation conditions. In case of $\text{Gd}_2\text{TiZrO}_7$, the random distribution of Ti and Zr atoms on the B-site increases the relative stability of the crystallized defect-fluorite structure, which is characterized by the random occupation of the cation sites by Gd, Ti or Zr. This random mixing of Zr with Ti increases the stochastic

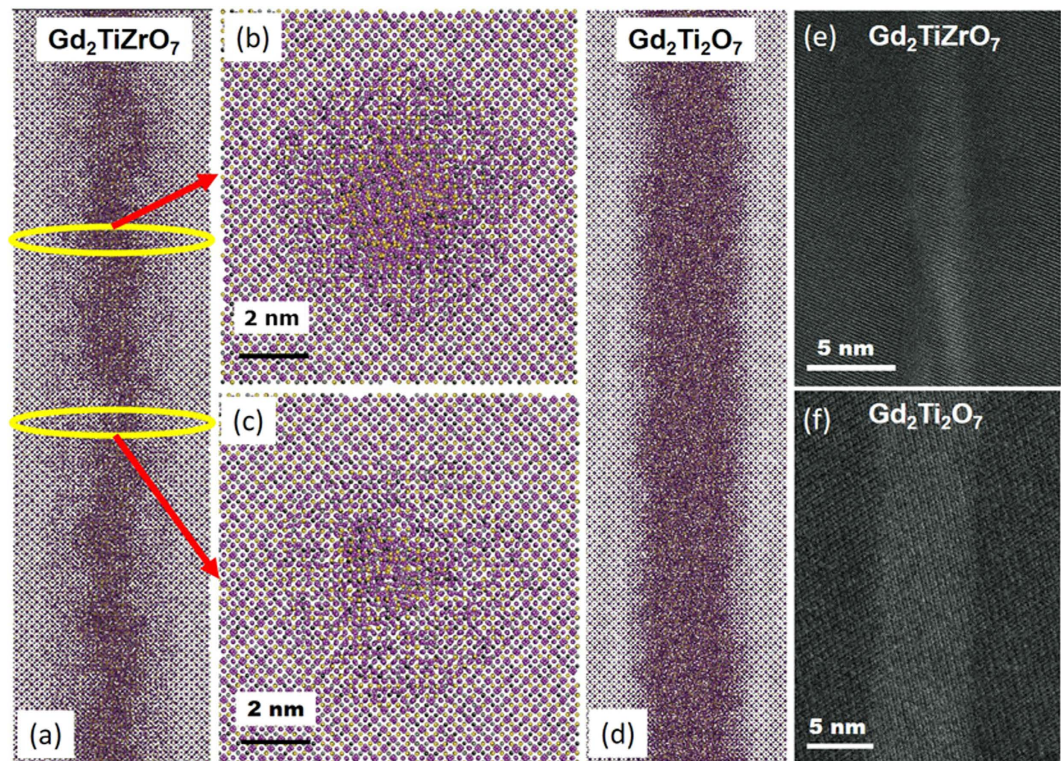


Figure 5. (a) A simulated ion track in $\text{Gd}_2\text{TiZrO}_7$ at 340 ps simulation time, illustrating the variation in the ion track diameter. (b,c) Cross sections of the ion track at two different depths, indicated in (a). The core diameter size is about 4 nm (b) and 2 nm (c). (d) A simulated ion track in $\text{Gd}_2\text{Ti}_2\text{O}_7$ at 340 ps simulation time, illustrating a uniform diameter ion track. (e) A cross-sectional BF image of ion track in $\text{Gd}_2\text{TiZrO}_7$. (f) A cross-sectional BF image of ion track in $\text{Gd}_2\text{Ti}_2\text{O}_7$.

nature of the local energy dissipation and initiates a competition between defect fluorite and amorphous phase formation^{2,23,24}. This competition between defect fluorite and amorphous phase formation during the crystallization process, which is maximized in the $\text{Gd}_2\text{ZrTiO}_7$ composition, is believed to be the primary driving force for the dramatic diametric variations in track morphology observed in this material. To provide a better insight, MD simulations for track formation in several $\text{Gd}_2\text{Zr}_{(2-x)}\text{Ti}_x\text{O}_7$ compositions (where $x = 0.4, 0.6, 1, 1.6$ and 2) are shown in Fig. 6 and demonstrate clearly the competition between defect-fluorite and amorphous phase formation as a function of the ratio of Zr and Ti atoms on the B site. Materials with a mix of Ti and Zr show more morphological variations in the formed tracks, while the tracks formed in $\text{Gd}_2\text{Ti}_2\text{O}_7$ and $\text{Gd}_2\text{Zr}_2\text{O}_7$ (not shown)¹⁶ appear more uniform and cylindrical.

In this work, we present a detailed study of dramatic diametric variations in the ion tracks induced by swift heavy ions (2.3 GeV Pb) in $\text{Gd}_2\text{TiZrO}_7$. Using atomic resolution depth-dependent HAADF imaging of ion tracks, we show the complexity of track formation in $\text{Gd}_2\text{TiZrO}_7$, where the variation of track diameter is as large as ~40% despite a constant electronic energy loss. By analyzing different ion tracks, it is concluded that these diameter fluctuations are due to the random distribution of Ti and Zr atoms on the B-site of crystal lattice, which locally modifies the energy dissipation and recrystallization processes. In particular, the competition between amorphous phase formation (favored by Ti atoms) and defect-fluorite phase formation (favored by Zr atoms) during the crystallization process induces the observed diametric fluctuations in track morphology.

Methods

Ion irradiation. Polycrystalline sample of $\text{Gd}_2\text{TiZrO}_7$ was prepared by annealing the densified pellets at 800 °C for 24 hrs. The grain size in the samples was ~3–4 μm, which is sufficiently large to negate any effect on bulk track formation^{8,13,25}. Also, the proximity of grain boundaries and the orientation of grains have negligible effects at such high electronic energy-loss^{8,25}. The samples were further polished to 40 μm thickness. These samples were irradiated at room temperature with 2.3 GeV energy ²⁰⁸Pb ions at the beamline X0 of the UNILAC linear accelerator at the GSI Helmholtz Center in Darmstadt, Germany. The ion fluence in the experiment was kept at $\sim 5 \times 10^{10}$ ions/cm² in order to create isolated ion tracks. The details of sample preparation and ion irradiation are elaborated elsewhere^{14,18}. The Stopping and Range of Ions in Matter code (SRIM-2013) was used to estimate the nuclear (S_n) and electronic (S_e) energy-loss, respectively, as a function of energetic ion penetration depth in $\text{Gd}_2\text{TiZrO}_7$.

STEM imaging. The plan-view STEM samples were prepared to analyze the morphology of ion tracks at a depth of ~10 μm from the irradiated surface. The samples for STEM analysis were prepared by

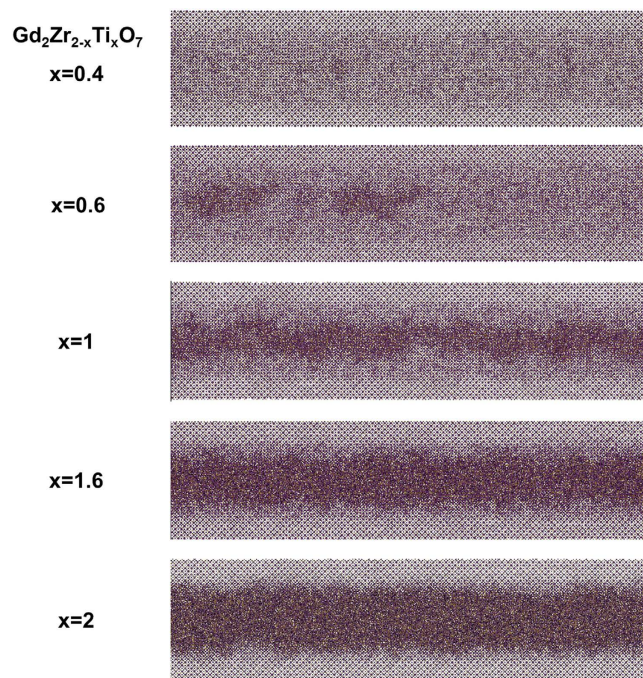


Figure 6. MD simulations of ion track formation in various $\text{Gd}_2\text{Zr}_{(2-x)}\text{Ti}_x\text{O}_7$ compositions. Conditions used for simulations are same as described in the methods section. Figure shows the competition between defect fluorite and amorphous phase transformation in the ion track as the effect of changing Zr:Ti ratio on the B atom site.

mechanically polishing the samples to a thickness of $\sim 10\ \mu\text{m}$, followed by ion milling in a liquid N_2 environment²⁶. In the mechanical polishing step, the samples were thinned by removing $\sim 25\ \mu\text{m}$ back side and $\sim 5\ \mu\text{m}$ from the irradiated surface. The ion milling was performed using ion guns on both sides of the samples. The samples for cross-sectional imaging were prepared by crushing the irradiated materials into fine powder and subsequently depositing onto a lacey carbon TEM grid. The HAADF and BF imaging was conducted in a 5th order aberration corrected STEM (Nion UltraSTEM 200) operating at 200 kV. The electron probe with 28 pA current was used in the experiment. HAADF images were obtained using a detector with an inner angle of 65 mrad. The BF images were collected with detector having ~ 15 mrad outer collection angle.

Molecular Dynamics simulations. For the MD simulations, the DL_POLY MD code was used²⁷. The system consists of about 1.2 million atoms and the MD box has $20\ \text{nm} \times 20\ \text{nm} \times 40\ \text{nm}$ length. We have used the Minervini and Grimes empirical potentials²⁸, joined with the short range ZBL potentials²⁹. The ZBL potentials were used for all atomic pairs. The energy deposition from the Pb ions is described by a Gaussian profile with a 2 nm standard deviation³⁰. The electron-phonon coupling efficiency is taken to be 0.45. The irradiation of the system was along the z direction under the NVE (constant-volume, constant-energy) ensemble at 300 K, following the equilibration of the system under the NPT (constant pressure, constant-temperature) ensemble. A Langevin thermostat was connected to the atoms contained in a layer of $10\ \text{\AA}$ along the x and y boundaries of the MD box to emulate the effect of energy dissipation into the sample.

References

- Meldrum, A., Boatner, L. A., White, C. W. & Ewing, R. C. Ion irradiation effects in nonmetals: formation of nanocrystals and novel microstructures. *Mat Res Innovat* **3**, 190, doi: 10.1007/s100190050003 (2000).
- Toulemonde, M. *et al.* *Ion Beam Science: Solved and Unsolved Problems* (The Royal Danish Academy of Sciences and Letters, 2006).
- Weber, W. J. *et al.* Synergy of elastic and inelastic energy loss on ion track formation in SrTiO_3 . *Sci. Rep.* **5**, 7726, doi: 10.1038/srep07726 (2015).
- Matzke, H. & Kinoshita, M. Polygonization and high burnup structure in nuclear fuels. *J. Nucl. Mater.* **247**, 108, doi: 10.1016/S0022-3115(97)00081-0 (1997).
- Sickafus, K. E. *et al.* Radiation tolerance of complex oxides. *Science* **289**, 748, doi: 10.1126/science.289.5480.748 (2000).
- Price, P. B. Advances in solid state nuclear track detectors. *Nucl. Tracks Radiat. Meas.* **22**, 9, doi: 10.1016/0969-8078(93)90007-Q (1993).
- Boscherini, M. *et al.* Radiation damage of electronic components in space environment. *Nucl. Instrum. Methods Phys. Res., Sect. A* **514**, 112, doi: 10.1016/j.nima.2003.08.091 (2003).
- Zhang, J. M. *et al.* Nanoscale phase transitions under extreme conditions within an ion track. *J. Mater. Res.* **25**, 1344, doi: 10.1557/Jmr.2010.0180 (2010).
- Wunsch, B. J. *et al.* Connection between oxygen-ion conductivity of pyrochlore fuel-cell materials and structural change with composition and temperature. *Solid State Ionics* **129**, 111, doi: 10.1016/S0167-2738(99)00320-3 (2000).
- Aidhy, D. S. *et al.* Fast ion conductivity in strained defect-fluorite structure created by ion tracks in $\text{Gd}_2\text{Ti}_2\text{O}_7$. *Sci Rep* **5**, 16297, doi: 10.1038/srep16297 (2015).

11. Machida, Y., Nakatsuji, S., Onoda, S., Tayama, T. & Sakakibara, T. Time-reversal symmetry breaking and spontaneous Hall effect without magnetic dipole order. *Nature* **463**, 210, doi: 10.1038/nature08680 (2010).
12. Besikiotis, V., Knee, C. S., Ahmed, I., Haugrud, R. & Norby, T. Crystal structure, hydration and ionic conductivity of the inherently oxygen-deficient $\text{La}_2\text{Ce}_2\text{O}_7$. *Solid State Ionics* **228**, 1, doi: 10.1016/j.ssi.2012.08.023 (2012).
13. Lang, M. *et al.* Single-ion tracks in $\text{Gd}_2\text{Zr}_{2-x}\text{Ti}_x\text{O}_7$ pyrochlores irradiated with swift heavy ions. *Phys. Rev. B* **79**, 224105, doi: 10.1103/PhysRevB.79.224105 (2009).
14. Lang, M. *et al.* Swift heavy ion track formation in $\text{Gd}_2\text{Zr}_{2-x}\text{Ti}_x\text{O}_7$ pyrochlore: Effect of electronic energy loss. *Nucl. Instrum. Methods Phys. Res., Sect. B* **336**, 102, doi: 10.1016/j.nimb.2014.06.019 (2014).
15. Jozwik-Biala, I. *et al.* Effect of combined local variations in elastic and inelastic energy losses on the morphology of tracks in ion-irradiated materials. *Acta Mater.* **61**, 4669, doi: 10.1016/j.actamat.2013.04.037 (2013).
16. Sattonnay, G. *et al.* Phase transformations induced by high electronic excitation in ion-irradiated $\text{Gd}_2\text{Zr}_x\text{Ti}_{(1-x)}\text{O}_7$ pyrochlores. *J. Appl. Phys.* **108**, 103512, doi: 10.1063/1.3503452 (2010).
17. Wang, J., Lang, M., Ewing, R. C. & Becker, U. Multi-scale simulation of structural heterogeneity of swift-heavy ion tracks in complex oxides. *J. Phys.: Condens. Matter* **25**, 135001, doi: 10.1088/0953-8984/25/13/135001 (2013).
18. Lang, M. *et al.* Structural modifications of $\text{Gd}_2\text{Zr}_{2-x}\text{Ti}_x\text{O}_7$ pyrochlore induced by swift heavy ions: Disorder and amorphization. *J. Mater. Res.* **24**, 1322, doi: 10.1557/jmr.2009.0151 (2011).
19. Weber, W. J., Duffy, D. M., Thomé, L. & Zhang, Y. The role of electronic energy loss in ion beam modification of materials. *Curr. Opin. Solid State Mater. Sci.* **19**, 1, doi: 10.1016/j.cossms.2014.09.003 (2015).
20. Pennycook, S. J. *et al.* Aberration-corrected scanning transmission electron microscopy: from atomic imaging and analysis to solving energy problems. *Philos. Trans. R. Soc., A* **367**, 3709, doi: 10.1098/rsta.2009.0112 (2009).
21. Jozwik-Biala, I. *et al.* HRTEM study of track evolution in 120-MeV U irradiated $\text{Gd}_2\text{Ti}_2\text{O}_7$. *Nucl. Instrum. Methods Phys. Res., Sect. B* **286**, 258, doi: 10.1016/j.nimb.2011.12.040 (2012).
22. Studer, F., Hervieu, M., Costantini, J. M. & Toulemonde, M. High resolution electron microscopy of tracks in solids. *Nucl. Instrum. Methods Phys. Res., Sect. B* **122**, 449, doi: 10.1016/S0168-583X(96)00575-7 (1997).
23. Dartyge, E. & Sigmund, P. Tracks of heavy ions in muscovite mica: Analysis of the rate of production of radiation defects. *Phys. Rev. B* **32**, 5429, doi: 10.1103/PhysRevB.32.5429 (1985).
24. Studer, F. & Toulemonde, M. Irradiation damage in magnetic insulators. *Nucl. Instrum. Methods Phys. Res., Sect. B* **65**, 560, doi: 10.1016/0168-583X(92)95105-Z (1992).
25. Zhang, J. *et al.* Enhanced radiation resistance of nanocrystalline pyrochlore $\text{Gd}_2\text{Ti}_{0.65}\text{Zr}_{0.35}\text{O}_7$. *Appl. Phys. Lett.* **94**, 243110, doi: 10.1063/1.3155855 (2009).
26. Sachan, R. *et al.* Structure and band gap determination of irradiation-induced amorphous nano-channels in LiNbO_3 . *J. Appl. Phys.* **117**, 135902, doi: 10.1063/1.4915932 (2015).
27. Todorov, I. T., Smith, W., Trachenko, K. & Dove, M. T. DL_POLY_3: new dimensions in molecular dynamics simulations via massive parallelism. *J. Mater. Chem.* **16**, 1911, doi: 10.1039/B517931A (2006).
28. Minervini, L., Grimes, R. W. & Sickafus, K. E. Disorder in Pyrochlore Oxides. *J. Am. Ceram. Soc.* **83**, 1873, doi: 10.1111/j.1151-2916.2000.tb01484.x (2000).
29. Ziegler, J. F., Biersack, J. P. & Ziegler, M. D. *SRIM, the stopping and range of ions in matter*. Available at: <http://www.srim.org> (Accessed: 16 July 2015).
30. Lang, M., Devanathan, R., Toulemonde, M. & Trautmann, C. Advances in understanding of swift heavy-ion tracks in complex ceramics. *Curr. Opin. Solid State Mater. Sci.* **19**, 39, doi: <http://dx.doi.org/10.1016/j.cossms.2014.10.002> (2015).

Acknowledgements

This work was supported by the US Department of Energy, Office of Science, Basic Energy Sciences, Materials Sciences and Engineering Division. A portion of this work was conducted at the Center for Nanophase Materials Sciences, which is a DOE Office of Science User Facility. The computer simulation used the resources of the National Energy Research Scientific Computing Center, supported by the US Department of Energy Office of Science under Contract No. DEAC02-05CH11231. The infrastructure of the GSI Helmholtzzentrum fuer Schwerionenforschung (Darmstadt, Germany) was used to do perform the irradiations.

Author Contributions

R.S. and W.J.W. initiated and coordinated the research. R.S. and M.F.C. performed the STEM imaging. M.L. and C.T. conducted the ion irradiation experiment. E.Z. performed the MD simulations. R.S., E.Z., Y.Z., M.F.C. and W.J.W. contributed in preparing the manuscript.

Additional Information

Supplementary information accompanies this paper at <http://www.nature.com/srep>

Competing financial interests: The authors declare no competing financial interests.

How to cite this article: Sachan, R. *et al.* Insights on dramatic radial fluctuations in track formation by energetic ions. *Sci. Rep.* **6**, 27196; doi: 10.1038/srep27196 (2016).



This work is licensed under a Creative Commons Attribution 4.0 International License. The images or other third party material in this article are included in the article's Creative Commons license, unless indicated otherwise in the credit line; if the material is not included under the Creative Commons license, users will need to obtain permission from the license holder to reproduce the material. To view a copy of this license, visit <http://creativecommons.org/licenses/by/4.0/>